J. Ocean Univ. China (Oceanic and Coastal Sea Research)
https://doi.org/10.1007/s11802-020-4021-4
ISSN 1672-5182, 2020 19 (2): 377-385
http://www.ouc.edu.cn/xbywb/
E-mail:xbywb@ouc.edu.cn

Strontium Isotope Compositions of Hydrothermal Barite from the Yonaguni IV: Insight into Fluid/Sediment Interaction and Barite Crystallization Condition

ZHANG Xia, ZHAI Shikui*, and YU Zenghui

Key Laboratory of Submarine Geosciences and Prospecting Techniques, *Ministry of Education*, *College of Marine Geosciences*, *Ocean University of China*, *Qingdao* 266100, *China*

(Received September 27, 2018; revised May 29, 2019; accepted September 16, 2019)

Abstract Hydrothermal barite is a typical low-temperature mineral formed during the mixing of hydrothermal fluid and seawater. Because of its extremely low solubility, barite behaves as a close system after crystallization and preserves the geochemical fingerprint of hydrothermal fluid. In this study, the elemental contents and Sr isotope compositions of hydrothermal barites from the Yonaguni IV were determined using electron microprobe and LA-MC-ICP-MS respectively. On these bases, the fluid/sediment interaction during the hydrothermal circulation and physicochemical condition of barite crystallization were discussed. Results show that the $^{87}Sr/^{86}Sr$ values of hydrothermal barites from the Yonaguni IV are apparently higher than those of the seawater and associated volcanic rocks, indicating the sufficient interaction between the hydrothermal fluid and overlying sediment. Monomineral Sr abundance shows large variations, reflecting the changes in barite growth rate during the fluid mixing. The mineralization condition in the Yonaguni IV was unstable. During the crystallization of barite, hydrothermal fluid and seawater mixed in varying degrees, with the proportions of hydrothermal fluid varied from 36% to 72%. The calculated crystallization temperatures range from 109 to 220℃. Sediment plays a critical role during the mineralization process in the Yonaguni IV and incorporation of sediment component into hydrothermal system was prior to barite crystallization and sulfide mineralization.

Key words strontium isotope; hydrothermal barite; fluid/sediment interaction; crystallization condition; Okinawa Trough

1 Introduction

Barite, a common hydrothermal mineral in the back-arc basin hydrothermal fields, is generally formed in the low-temperature stage of mineralization (Tivey *et al*., 1990). As a key structural component to hydrothermal edifices, its occurrence and abundance can affect hydrothermal deposit morphology, chimney growth and the retention of metals within a deposit (Tivey and Delaney, 1986; Hannington *et al*., 1995). Hydrothermal barite was formed during the mixing of barium-rich fluid and sulfate-rich seawater (Damn, 1990; Hannington *et al*., 2005; Humphris and Bach, 2005). Because of its extremely low solubility in seawater, barite behaves as a close system and is not prone to diagenetic alteration after crystallization (Averyt and Paytan, 2003; Widanagamage *et al*., 2014), preserving the geochemical fingerprint of hydrothermal fluid. Thus, geochemical compositions of barite can indicate the regional mineralization characteristics and physicochemical conditions of barite crystallization (Jamieson *et al*., 2016).

Due to the common substitution of Sr to Ba during barite crystallization under hydrothermal condition, the contents of Sr are generally high (reach up to 4.6%; Hanor, 2000) in natural barite, which makes it possible to determine the Sr isotope compositions in barite. Strontium isotope compositions of barite in hydrothermal fields have been studied sufficiently, which revealed the fluid mixing process, source of mineralization materials and fluid/sediment interaction (Marchev *et al*., 2002; Paytan *et al*., 2002; Cardellach *et al*., 2003; Noguchi *et al*., 2011; Staude *et al*., 2011; Jamieson *et al*., 2016). While the Sr isotope research about hydrothermal barite in the Okinawa Trough is extremely poor, only Noguchi *et al*. (2011) reported the Sr isotope compositions of hydrothermal barite from the JADE hydrothermal field. Up to now, no Sr isotope research about hydrothermal barite in the Southern Okinawa Trough has been carried out. Yonaguni IV hydrothermal field is located in the southern Okinawa Trough. Barite-rich Ba-Zn-Pb type hydrothermal deposit was developed in this region, which provides the perfect sample for Sr isotope compositions study of hydrothermal barite. In this study, we report the first data on elemental contents and Sr isotope compositions of barites from the Yonaguni IV. On these bases, the hydrothermal fluid/sediment interaction during the hydrothermal circulation and physicochemical

* Corresponding author. E-mail: zhai2000@ouc.edu.cn

condition of barite crystallization were discussed.

2 Geological Setting

The Okinawa Trough, an important part of the East China Sea, is a tectonically active intracontinental back-arc basin generated by the subduction of the Philippine plate under the Eurasian continent (Halbach *et al*., 1993). The heat-flow values in the Okinawa Tough are extremely high. Since the first discovery of hydrothermal activity in the middle Okinawa Trough in 1984, a large number of hydrothermal fields have been reported gradually.

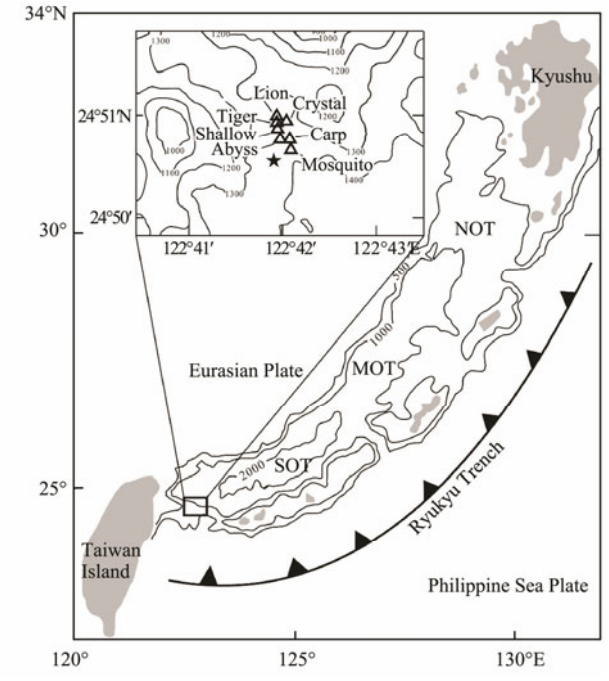

Fig.1 Sampling locations and bathymetric map of the Okinawa Trough (after Gena *et al*., 2013). The triangles are the major hydrothermal vents in this field and the pentagram is the sample location of this study.

Yonaguni IV hydrothermal field is located in the southernmost part of the Okinawa Trough (Matsumoto *et al*., 2002; Fig.1). Venting sites in this field are aligned along a 1000 m-long and 500 m-wide elongated valley which was interpreted by Suzuki *et al*. (2008) to represent a fault that may have controlled the fluid pathways to the seafloor. The valley is surrounded by several seamounts with the maximum water depth up to 1400 m. The local topography within the valley is almost flat and the seafloor is covered by thick brown sediments which are cemented by native sulfur, quartz and barite indicating the influence of hydrothermal fluid. Seven hydrothermal vents (lion, crystal, tiger, swallow, abyss, crap and mosquito) were discovered in this field (Gena *et al*., 2005), with the highest fluid temperature about 330℃ (Inagaki *et al*., 2006; Suzuki *et al*., 2008; Nunoura and Takai, 2009). Between the Tiger and Swallow sites, liquid CO_2 droplet was observed emerging from the seafloor (Konno *et al*., 2006). Suzuki *et al*. (2008) studied the mineralogy of hydrothermal chimney from lion, crystal, tiger and swallow and recognized five types of hydrothermal deposits: i) anhydrite-rich chimneys; ii) massive Zn-Pb-Cu sulfides; iii) Ba-As chimneys; iv) Mn-rich chimneys; v) pavement, silicified sediment. They proposed the diverse series of mineralization was the result of phase separation.

3 Sampling and Analytical Methods

The hydrothermal deposit sample studied in this paper was grabbed from the Yonaguni IV hydrothermal field (122°41′55″E, 24°50′26″N) during the HOBAB3 cruise in 2014 with water depth of 1390 m. Mineralogically, the sample is similar to the Ba-As chimneys recognized by Suzuki *et al*. (2008) in this region, which mainly consist of barite, sphalerite and galena.

The hydrothermal sample was firstly ultrasonic cleaned in distilled water for 45 min to remove the effect of seawater and sediment contamination. Then the dried sample was cut into thin sections and doubly-polished for electron microprobe and LA-MC-ICP-MS analyses. The elemental abundances of barites were determined in the Key Laboratory of Submarine Geosciences and Prospecting Techniques, Ministry of Education, by JXA-8230 Electron Microprobe. The instrument parameters were acceleration voltage of 15 kV, a beam current of 20 nA and beam diameter of 3 μm. The Sr isotope compositions of hydrothermal barites were analyzed in State Key Laboratory of Isotope Geochemistry, Guangzhou Institute of Geochemistry, Chinese Academy of Sciences using Neptune Plus LA-MC-ICP-MS and the analyzing method followed Zhang *et al*. (2018a). The laser parameters were set as follow: beam diameter, 33 μm; repetition rate, 6 Hz; energy density, 4 J cm^{-2}. Helium was chosen as the carrier gas (800 mL min^{-1}). Each analysis consisted of 250 cycles with an integration time of 0.262 s per cycle. The first 30 s was used to detect the gas blank with the laser beam off, followed by 30 s laser ablation for sample signals collection with laser beam on. During the measurement of this study, the gas blank of ^{83}Kr and ^{88}Sr were less than 2.5 mv and 0.5 mv. The interferences of ^{84}Kr and ^{86}Kr on ^{84}Sr and ^{86}Sr were corrected by subtracting gas blank from the raw time-resolved signal intensities. Seven Faraday cups, on a Neptune Plus MC-ICP-MS instrument, were used to receive the signals on m/z 82, 83, 84, 85, 86, 87 and 88 simultaneously for the Sr isotope analysis of hydrothermal barite. ^{85}Rb was used to correct the interference of ^{87}Rb on ^{87}Sr with a natural ^{85}Rb/^{87}Rb = 2.593 (Catanzaro *et al*., 1969). The instrumental mass fraction of ^{87}Sr/^{86}Sr was corrected to ^{86}Sr/^{88}Sr = 0.1194 with an exponential law. Finally, the residual analytical biases of ^{87}Sr/^{86}Sr were corrected with a relationship between the deviations of ^{87}Sr/^{86}Sr from the reference values.

4 Results

Barites within hydrothermal deposit sample from the Yonaguni IV occur as two types of crystal habits, well-formed tabular and needle-like crystal, with sizes varying from 50 to 300 μm. Later-formed sulfide minerals fill in

the interface of barite (Fig.2). The analysis results of mononmineral elemental abundance (Table 1) show that the contents of BaO in the barite are relatively homogeneous (62.59% – 64.81%), while the contents of SrO have a large variation between 0.30% and 2.54%. The contents of CaO are extremely low (lower than 0.4%), indicating that the substitution of Ca to Ba was weak during the barite crystallization.

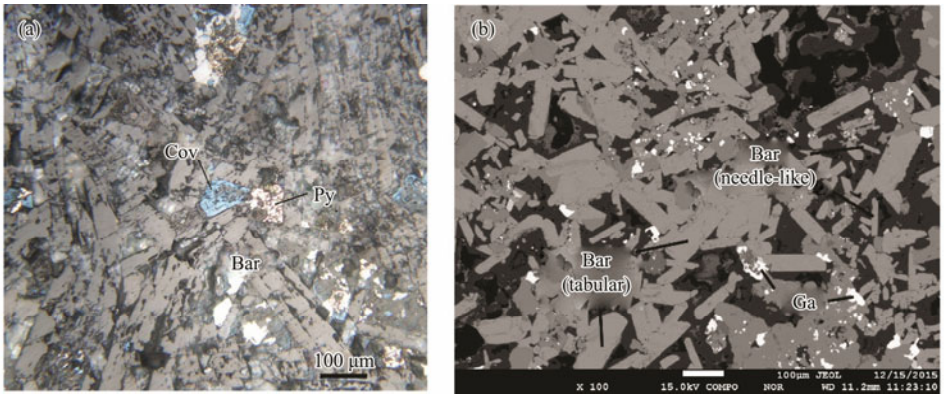

Fig.2 (a) Reflection light and (b) backscatter scanning photomicrographs of hydrothermal deposit from the Yonaguni IV. Bar, barite; Cov, covellite; Ga, galena; Py, pyrite.

Table 1 Electron microprobe analysis results of elemental contents across single barite

Analysis#		BaO (%)	SO_3 (%)	SrO (%)	MgO (%)	CaO (%)	Al_2O_3 (%)	FeO (%)	Total
Grain1	1	64.81	33.48	0.72	0.02	0.07	0.03	0.01	99.14
	2	64.40	33.68	1.39	0.08	0.12	0.06	–	99.73
	3	64.77	33.96	0.73	0.01	0.09	0.10	–	99.66
	4	64.09	33.59	1.47	0.03	0.12	0.09	0.01	99.40
	5	64.70	33.85	0.89	0.03	0.07	0.06	–	99.60
	6	62.68	33.86	2.02	–	0.21	0.06	0.03	98.86
	7	62.61	34.18	1.78	0.03	0.38	0.03	–	99.01
	8	62.59	33.25	2.54	0.03	0.30	0.08	0.05	98.84
	9	62.78	33.87	2.53	0.08	0.30	0.04	0.04	99.64
	10	63.55	33.14	2.40	0.01	0.30	0.08	–	99.48
Grain2	1	64.61	33.63	0.30	0.05	0.05	0.03	–	98.67
	2	64.67	33.77	0.44	–	0.05	0.04	–	98.97
	3	62.92	34.29	2.01	0.01	0.37	0.04	0.03	99.67
	4	62.94	34.15	2.24	0.04	0.40	0.07	–	99.84
	5	63.29	33.67	1.95	0.01	0.32	0.06	0.04	99.34
	6	63.05	33.82	1.98	0.21	0.38	0.05	–	99.49

Note: '–' means lower than detected limits.

The Sr isotope compositions of barites show large variation, with the $^{87}Sr/^{86}Sr$ values varying from 0.71284 to 0.71749 (Table 2), which are apparently higher than those of seawater (0.7092; Butterfield *et al*., 2001) and regional volcanic rocks (0.704035–0.708635; Guo *et al.*, 2018), but fall between the values of seawater and Yonaguni IV sediment (0.72212; Dou *et al*., 2016). Compared with other hydrothermal fields, barites from the Yonaguni IV also have apparently higher $^{87}Sr/^{86}Sr$ which are the highest values reported up till now (Fig.3).

5 Discussion

5.1 Hydrothermal Fluid/Sediment Interaction

Strontium isotope compositions of barites from the sediment-starve hydrothermal fields generally lie between those of basement rocks and seawater (Fouquet *et al*., 1993), reflecting the mixing of magmatic and seawater-derived Sr. While the $^{87}Sr/^{86}Sr$ values of hydrothermal barites from the Yonaguni IV are apparently higher than those of seawater and associated volcanic rocks, but fall between the values of seawater and Yonaguni IV sediment. These values suggest the interaction between hydrothermal fluid and local sediment during the hydrothermal circulation. Chiba *et al*. (1993) reported that the $^{87}Sr/^{86}Sr$ value in the Minami-Ensei Knoll hydrothermal fluid was higher than those in regional volcanic rocks and seawater and proposed that the composition of hydrothermal fluid in this region was affected by the interaction with sediment during the late stage of hydrothermal circulation. Noguchi *et al*. (2011) found the $^{87}Sr/^{86}Sr$ values of hydrothermal barites from the Hakurei field were higher than that of seawater and attributed it to the interaction between hydrothermal fluid and sediment as well. Yonaguni IV hydrothermal field is covered by thick terrigenous sediment (Dou *et al*., 2016), which may interact with hydrothermal fluid during

the hydrothermal circulation. Suzuki *et al*. (2008) detected large amounts of NH_4^+ in the Yonaguni IV hydrothermal fluid and found the hydrothermal-altered sediment, providing the incontrovertible evidences for fluid/sediment interaction in this field. Thus, we propose that the abnormally high $^{87}Sr/^{86}Sr$ values of hydrothermal barites from the Yonaguni IV field are the result of fluid/sediment interaction. Fluid/sediment interaction will elevate the Sr isotope ratio in the hydrothermal fluid and lead to the high $^{87}Sr/^{86}Sr$ values of barites. The high Sr isotope ratios of the Yonaguni IV barites imply that the fluid/sediment interaction in this region is very sufficient and sediment might play a critical role during the hydrothermal mineralization.

Table 2 LA-MC-ICP-MS analysis results of Sr isotope compositions within the hydrothermal barites and standard references

Analysis#	^{85}Rb intensity	^{88}Sr intensity	$^{87}Rb/^{86}Sr$	$^{87}Sr/^{86}Sr$	%HF	T (℃)
L1	0.003560	1.53	0.002867	0.71504 ± 0.00007	54	165
L2	0.000499	6.78	0.000216	0.71436 ± 0.00005	48	149
L3	0.000379	6.45	0.000159	0.71395 ± 0.00009	45	139
L4	0.000360	7.20	0.000101	0.71331 ± 0.00004	40	122
L5	0.000214	1.55	0.000284	0.71627 ± 0.00008	63	194
L6	0.000262	2.25	0.000275	0.71412 ± 0.00006	46	143
L7	0.000179	0.56	0.000384	0.71640 ± 0.00018	64	197
L8	0.000405	1.96	0.000470	0.71692 ± 0.00010	68	208
L9	0.000330	7.45	0.000116	0.71360 ± 0.00005	42	129
L10	0.000331	5.30	0.000160	0.71462 ± 0.00005	50	155
L11	0.000237	2.34	0.000212	0.71749 ± 0.00019	72	220
L12	0.000287	4.99	0.000118	0.71367 ± 0.00005	43	131
L13	0.000701	12.62	0.000176	0.71284 ± 0.00003	36	109
L14	0.000299	5.58	0.000137	0.71484 ± 0.00006	52	160
L15	0.000387	7.45	0.000148	0.71360 ± 0.00004	42	129
L16	0.000346	4.23	0.000209	0.71498 ± 0.00005	53	164
NKT-1G (n = 9)				0.70353 ± 0.00005		
Coral (n = 9)				0.70917 ± 0.00003		

Notes: NKT and Coral are the standard references of Sr isotope. The tested average $^{87}Sr/^{86}Sr$ values in this paper were consistent within errors with the reported value in Christensen *et al*. (1995) and Elburg *et al.* (2005), demonstrating that the $^{87}Sr/^{86}Sr$ values we measured by LA-MC-ICP-MS are accurate. %HF means the proportions of hydrothermal fluid; T means crystallization temperature of hydrothermal barite.

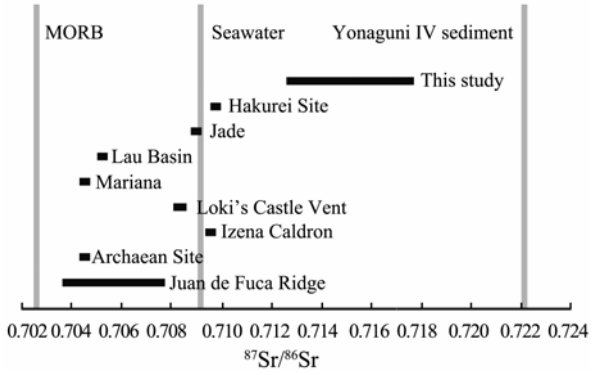

Fig.3 Strontium isotope compositions of hydrothermal barites from the modern hydrothermal fields. Juan de Fuca Ridge (Jamieson *et al*., 2016); Archaean Site, Izena Caldron, Hakurei Site (Noguchi *et al*., 2011); Loki's Castle Vent (Eickmann *et al*., 2014); Mariana (Paytan *et al*., 1993); Lau Basin (Fouquet *et al*., 1993); Jade (Marumo and Hattori, 1999).

5.2 Crystallization Condition of Barite in the Yonaguni IV

5.2.1 Factors controlling Sr abundances in the barite

It's very common that Sr substitutes Ba into crystal lattice of barite in natural systems, thus, the contents of Sr in barite are generally high (Hanor, 2000). Under hydrothermal environment, trace elements substitution within crystals is controlled by the composition of hydrothermal fluid, pressure, temperature and crystal growth rate (Sasaki and Minato, 1983; Hannington and Scott, 1988; Averyt and Paytan, 2003). Laboratory researches demonstrated that substitution of Sr into barite crystal increases with fluid temperature (Hanor, 2000; Averyt and Paytan, 2003). Alternatively, Shikazono *et al*. (2012) and Jamieson *et al*. (2016) linked increase Sr partitioning to higher degrees of saturation and fast crystal growth. Meanwhile, all of these researches have excluded the influence of hydrothermal fluid compositions on Sr contents in hydrothermal barite. Thus, the fluid source is not the controlling factors of Sr contents in barite. The elemental contents in monocrystal of barite show that the contents of Sr in barite have a large variation from the core to rim (Fig.4), demonstrating that the mineralization condition (fluid temperature or crystal growth rate) changed greatly during the barite crystallization, which is consistent with the conclusion obtained from the mineralogy study by Zhang *et al.* (2018b).

In the plots of ^{88}Sr intensity versus $^{87}Sr/^{86}Sr$ values (Fig.5), hydrothermal barites from the Yonaguni IV are aligned along a hyperbola, which is the typical characteristic of two end-members mixing (Faure, 1986), *i.e*., seawater (with high Sr content and low $^{87}Sr/^{86}Sr$ values) mixed with hydrothermal fluid (with low Sr content and high $^{87}Sr/^{86}Sr$). This demonstrates that the fluid mixing is

the major cause of the variation in Sr contents and $^{87}Sr/^{86}Sr$ values of barites from the Yonaguni IV. Previous researches (Hanor, 2000; Averyt and Paytan, 2003) demonstrated that mineralization fluid temperature decreased with the enhancing of fluid mixing, which will restrain the substitution of Sr to Ba and lower the Sr contents in barite. While the Sr contents (*i.e.*, ^{88}Sr intensity) in the barites from the Yonaguni IV increase with the fluid mixing degrees (Fig.5), which is contradictory to fluid temperature-controlled substitution of Sr to Ba. In this way, the change in barite crystal growth rate during the fluid mixing is the cause of Sr contents variation. Thus, although the mixing between hydrothermal fluid and seawater will lead to the changes both in fluid temperature and barite crystal growth rate, the fluid temperature change is apparently not the cause of Sr contents variation in the Yonaguni IV barites. Besides, it's noteworthy that the contents of Sr in barites show a decrease trend from the core to rim (Fig.4), which indicates that the fluid mixing degrees decreased during the barite crystallization and crystal growth rate reduced from the early to late stage. This is consistent with the growth stages of hydrothermal chimney: in the early stage of hydrothermal activity, the fluid mixing was intensive, causing the fast crystallization of barite and large amounts of Sr substituted Ba into crystals; with the development of hydrothermal activity, the chimney sealed gradually, restraining the fluid mixing and decreasing the growth rate of barite, Sr contents reduced as a result.

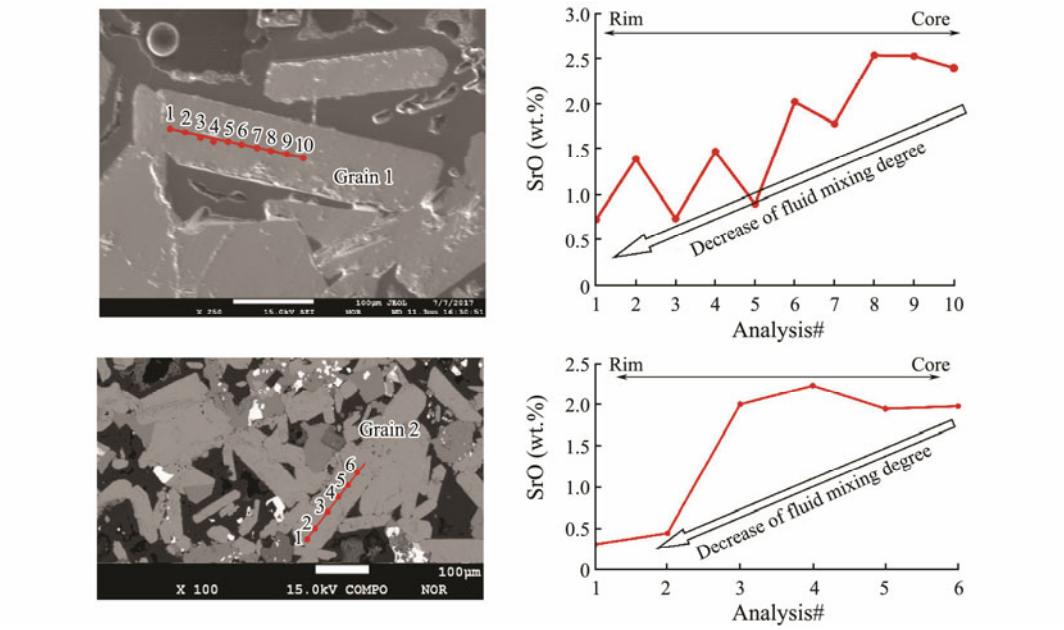

Fig.4 Electron microprobe analysis results of SrO contents across single barite.

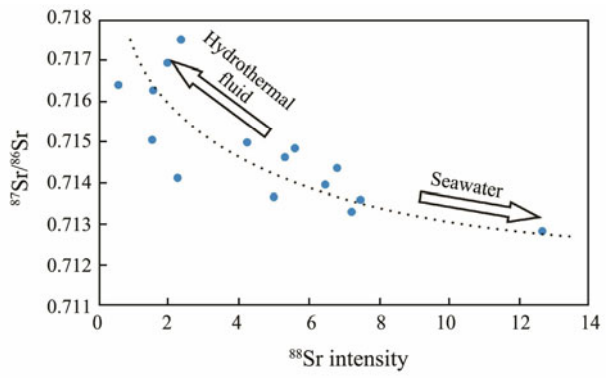

Fig.5 The $^{87}Sr/^{86}Sr$ *versus* ^{88}Sr intensity diagram of hydrothermal barites from the Yonaguni IV. The dotted line is simulated hyperbola which indicates the mixing of two end-member fluids (Faure, 1986). We propose that the two end-members are seawater ($Sr_{SW}=87\,\mu mol\,kg^{-1}$; $^{87}Sr/^{86}Sr=0.7092$; Seyfried *et al.*, 2003) and sediment-influenced hydrothermal fluid ($Sr_{HF}=61\,\mu mol\,kg^{-1}$; $^{87}Sr/^{86}Sr=0.72212$; Kishida *et al.*, 2004; Dou *et al.*, 2016). Here Sr_{SW} and Sr_{HF} are Sr concentrations of seawater and hydrothermal fluid respectively.

5.2.2 Sources of Ba

The source of Ba^{2+} is a key factor for barite crystallization. Barite contents are generally low in hydrothermal fields developed in the mid-ocean ridge due to the substrates being usually Ba-poor mid-ocean ridge basalts (Noguchi *et al.*, 2011). In immature back-arc basin hydrothermal fields, the contents of barite are generally high for the substrates are Ba-rich felsic volcanic rocks which provide a large amount of Ba^{2+} to the hydrothermal systems (Noguchi *et al.*, 2011; Jamieson *et al.*, 2016). In addition, the dehydration of subducted slab can add soluble Ba ion into the magma during plate subduction, which further elevated the Ba^{2+} abundances in the substrates (McCulloch and Gamble, 1991; You *et al.*, 1996). Yonaguni IV hydrothermal field is hosted by subduction component-influenced felsic volcanic rocks (Guo *et al.*, 2017, 2018; Zhang *et al.*, 2019a), which can provide large amounts of Ba^{2+} to the hydrothermal system and facilitate the crystallization of barite. Besides, the Yonaguni IV is covered by thick sediment which can also contribute abundant Ba^{2+} to the hydrothermal fluid during the

fluid/sediment interaction (Noguchi *et al*., 2011).

5.2.3 Fluid mixing

Sr isotopes cannot fractionate below 400℃ or during barite crystallization (Matter *et al*., 1987), therefore, strontium isotope compositions of barite record the isotope ratio of the mineralization fluid (Staude *et al*., 2011). The hydrothermal fluid/sediment interaction occurred during the hydrothermal circulation in the Yonaguni IV. Kuhn *et al*. (2003) proposed that if hydrothermal fluid/sediment interaction reached equilibration, the $^{87}Sr/^{86}Sr$ value of fluid should be equivalent to those of the sediments. We assumed that fluid/sediment interaction reached Sr isotope fractionation equilibration in the Yonaguni IV and took the average $^{87}Sr/^{86}Sr$ value of Southern Okinawa sediment (0.72212, $n=22$; Dou *et al*., 2016) as the Sr isotope composition of hydrothermal fluid. Then the relative contribution of hydrothermal fluid and seawater in the mixing fluid can be quantified by applying a two component mixing model:

$$\%HF = 100 \times Sr_{SW}((^{87}Sr/^{86}Sr)_{SW} - (^{87}Sr/^{86}Sr)_{BA}) / (Sr_{SW}((^{87}Sr/^{86}Sr)_{SW} - (^{87}Sr/^{86}Sr)_{BA}) + Sr_{HF}((^{87}Sr/^{86}Sr)_{BA} - (^{87}Sr/^{86}Sr)_{HF}),$$

where %HF is the proportion of hydrothermal fluid (with the remaining proportion being seawater), Sr_{SW} and Sr_{HF} are the Sr concentrations of seawater (87 μmol kg^{-1}; Seyfried *et al*., 2003) and hydrothermal fluid (61 μmol kg^{-1}; Kishida *et al*., 2004), respectively, and ($^{87}Sr/^{86}Sr)_{SW}$, ($^{87}Sr/^{86}Sr)_{BA}$ and ($^{87}Sr/^{86}Sr)_{HF}$ are Sr isotope ratios for seawater ($^{87}Sr/^{86}Sr = 0.7092$; Seyfriedet *et al*., 2003), barite and hydrothermal fluid ($^{87}Sr/^{86}Sr = 0.72212$).

Calculations show that hydrothermal fluid and seawater mixed in different proportions during the barite crystallization. The contribution of hydrothermal fluid component in the mixing fluid varied from 36% to 72% (Table 2), which further demonstrates that the mineralization condition in the Yonaguni IV is unstable and physiochemical condition of mixing fluid changes greatly during the mineralization process.

5.2.4 Crystallization temperature of hydrothermal barite

Hydrothermal barite is formed during the mixing of hydrothermal fluid and seawater (Damm, 1990; Hannington *et al*., 2005; Humphris and Bach, 2005). Thus, its crystallization temperature can be inferred using a linear thermal mixing relationship:

$$T_{BA} = xT_{HF} + (1-x)T_{SW},$$

where T_{BA} is the crystallization temperature of barite in degrees Celsius, T_{HF} and T_{SW} are the temperature of end-member hydrothermal fluid (310℃; Seyfried *et al*., 2003) and seawater (2℃; Glasby and Notsu, 2003; Suzuki *et al*., 2008), and x is the fraction of hydrothermal fluid in the mixture.

Results show that the crystallization temperatures of hydrothermal barite in the Yonaguni IV vary from 109 to 220℃, which indicates that the temperature of mixing fluid changed greatly during the barite precipitation and the mineralization condition is unstable. Due to the fluid temperature within a chimney is controlled not only by the mixing between hydrothermal fluid and seawater, but also by conductive cooling of hydrothermal fluid (Jamieson *et al*., 2016); the temperature calculated by the formula should be a little higher than the true crystallization temperature of barite.

5.2.5 Fluid saturation

Crystallographic features of barite reflect the physiochemical condition of hydrothermal fluid (Judat and Kind, 2004; Li *et al*., 2007; Feng and Roberts, 2011). Dendritic crystals grow quickly from the highly saturated fluid (Turcotte and Brown, 1997), while well-formed crystals grow slowly at lower saturation (Shikazono, 1994). The barites from the Yonaguni IV occur as two types of crystal, well-formed tabular and needle-like crystal (Fig.2), which were formed in different stages of mineralization. In the early stage, the fluid mixing was intensive and high saturation of $BaSO_4$ resulted in fast crystallization of the dendritic barite. With the development of hydrothermal activity, the chimney sealed gradually restraining the fluid mixing and lowering the $BaSO_4$ saturation in the fluid, barite crystalized as well-formed tabular as a result (Paytan *et al*., 2002; Ray *et al*., 2014).

In conclusion, the mineralization environment is unstable in the Yonaguni IV. During the barite crystallization, hydrothermal fluid mixed with seawater in different proportions, which led to the large variation in barite crystallization temperature, crystallographic features, Sr contents and $^{87}Sr/^{86}Sr$ values.

5.3 New Insight into Mineralization Material Source

According to the traditional hydrothermal leaching model, ore forming metals are mainly derived from the reaction between seawater and basement rocks at high temperature (Bischoff and Dickson, 1975; Humphris and Thompson, 1978; Mottl and Holland, 1978). Sediment may contribute a part of mineralization material in sediment covered hydrothermal fields (Lehuray *et al*., 1988; Zierenberg *et al*., 1993; Cousens *et al*., 2002; Zeng *et al*., 2017; Zhang *et al*., 2019b). With the deepening of research, importance of contribution from magmatic fluid to the hydrothermal systems has been realized recently (Yang and Scott, 1996; Kamenetsky *et al*., 2001). Wang *et al*. (2018) reviewed the results of previous researches and put forward the ‘double diffusive convection model’ which emphasized the contribution of both water/rock reaction and magmatic fluid. In the above models, sediment contribution to the hydrothermal systems is put on

the back burner. The hydrothermal barite from the Yonaguni IV has extremely high $^{87}Sr/^{86}Sr$, implying that sediment plays a critical role during the mineralization process. Sr isotope compositions of barite from other hydrothermal fields are generally fall between those of basement rocks and seawater (*e.g*., Fouquet *et al*., 1993), reflecting the mixing of magmatic and seawater-derived strontium. The measured $^{87}Sr/^{86}Sr$ values of barites in this study are apparently higher than the values of regional volcanic rocks and seawater but lie between those of seawater and Yonaguni IV sediment, which indicates that the hydrothermal fluid in the Yonaguni IV sufficiently interacted with the overlying sediment during the hydrothermal circulation. In this process, sediment may contribute a large amount of mineralization material to the hydrothermal system.

Previous researches have demonstrated that the mineralization characteristics in the Yonaguni IV are apparently different from those in the middle and northern Okinawa (Gena *et al*., 2013). For instance, Pt-rich bismuthinite is found in the Yonaguni IV and the Platinum group elements mineralization is generally associated with sediment (Hodge *et al*., 1986). Yonaguni IV hydrothermal field is covered by thick terrigenous sediment which may be the major source of Pt for Pt-rich bismuthinite. The hydrothermal deposit sample in this paper is Ba-Zn-Pb type and the barite contents are high up to 50%, such large amounts of barite require adequate supply of Ba^{2+}, while mere water/rock reaction can hardly satisfy the requirement. Sediment is rich in Ba^{2+}, which can provide large amounts of Ba^{2+} to the hydrothermal system during the fluid/sediment interaction. All the evidences above indicate that the hydrothermal deposit from the Yonaguni IV is seemingly different from the VHMS (volcanic-hosted massive sulfides) ores. Sediment plays a critical role during the mineralization process and probably is the major source of mineralization material. Moreover, fluid/sediment interaction changed the compositions of Yonaguni IV hydrothermal fluid greatly, especially in the Sr contents and $^{87}Sr/^{86}Sr$ values. This sediment-influenced fluid (with abnormally high $^{87}Sr/^{86}Sr$ values) mixing with seawater caused the crystallization of the hydrothermal barites. Thus, incorporation of the sediment component into the hydrothermal system was prior to the barite crystallization and sulfide mineralization.

6 Conclusions

1) The hydrothermal fluid sufficiently interacted with the sediment during mineralization process in the Yonaguni IV, which led to the apparently higher $^{87}Sr/^{86}Sr$ values of barites.

2) The mineralization environment is unstable in the Yonaguni IV. During the barite crystallization, hydrothermal fluid mixed with seawater in different proportions causing the large variation in barite crystallization temperature, crystallographic features, Sr contents and $^{87}Sr/^{86}Sr$ values.

3) The hydrothermal deposit from the Yonaguni IV is largely different from the VHMS ores. Sediment plays a critical role during the mineralization process.

Acknowledgements

This study is financially supported by the National Basic Research Program of China (No. 2013CB429702). We thank the two anonymous reviewers for their helpful comments in the early version of the paper.

References

Averyt, K. B., and Paytan, A., 2003. Empirical partition coefficients for Sr and Ca in marine barite: Implications for reconstructing seawater Sr and Ca concentrations. *Geochemistry, Geophysics, Geosystems*, **4** (5): 241-258.

Bischoff, J. L., and Dickson, F. W., 1975. Seawater-basalt interaction at 200℃ and 500 bars: Implications for origin of seafloor heavy-metal deposits and regulation of seawater chemistry. *Earth & Planetary Science Letters*, **25** (3): 385-397.

Butterfield, D. A., Nelson, B. K., Wheat, C. G., Mottl, M., and Roe, K., 2001. Evidence for basaltic Sr in midocean ridge-flank hydrothermal systems and implications for the global oceanic Sr isotope balance. *Geochimica et Cosmochimica Acta*, **65** (22): 4141-4153.

Cardellach, E., Canals, A., and Grandia, F., 2003. Recurrent hydrothermal activity induced by successive extensional episodes: The case of the Berta F-(Pb-Zn) vein system (NE Spain). *Ore Geology Reviews*, **22** (1): 133-141.

Catanzaro, E. J., Murphy, T. J., Garner, E. L., and Shields, W. R., 1969. Absolute isotopic abundance ratio and atomic weight of terrestrial rubidium. *Journal of Research of National Bureau of Standards*, **73** (5): 511-516.

Chiba, H., Nakashima, K., Gamo, T., Ishibashi, J., Tsunogai, U., and Sakai, H., 1993. Hydrothermal activity at the Minami-Ensei Knoll, Okinawa Trough: Chemical characteristics of hydrothermal solutions. *Proceeding of the JAMSTEC Symposium Deep Sea Research*, **9**: 271-282 (in Japanese with English abstract).

Christensen, J. N., Halliday, A. N., Lee, D. C., and Hall, C. M., 1995. *In situ* Sr isotopic analysis by laser ablation. *Earth & Planetary Science Letters*, **136** (1): 79-85.

Cousens, B. L., Blenkinsop, J., and Franklin, J. M., 2002. Lead isotope systematics of sulfide minerals in the middle valley hydrothermal system, northern Juan de Fuca Ridge. *Geochimica et Cosmochimica Acta*, **3** (5): 1-16.

Damm, K. L. V., 1990. Seafloor hydrothermal activity: Black smoker chemistry and chimneys. *Annual Review of Earth & Planetary Sciences*, **18** (1): 173-204.

Dou, Y., Yang, S., Shi, X., Clift, P. D., Liu, S., Liu, J., Li, C., Bi, L., and Zhao, Y., 2016. Provenance weathering and erosion records in southern Okinawa Trough sediments since 28 ka: Geochemical and Sr-Nd-Pb isotopic evidences. *Chemical Geology*, **425**: 93-109.

Eickmann, B., Thorseth, I. H., Peters, M., Strauss, H., Brocker, M., and Pedersen, R. B., 2014. Barite in hydrothermal environments as a recorder of subseafloor processes: A multiple-isotope study from the Loki's Castle vent field. *Geobiology*, **12** (4): 308-321.

Elburg, M., Vroon, P., Wagt, B. V. D., and Tchalikian, A., 2005. Sr and Pb isotopic composition of five USGS glasses (BHVO-2G, BIR-1G, BCR-2G, TB-1G, NKT-1G). *Chemical Geology*, **223** (4): 196-207.

Faure, G., 1986. *Principles of Isotope Geology*. John Wiley and Sons Inc., Chichester, 1-1207.

Feng, D., and Roberts, H. H., 2011. Geochemical characteristics of the barite deposits at cold seeps from the northern Gulf of Mexico continental slope. *Earth & Planetary Science Letters*, **309** (1): 89-99.

Fouquet, Y., 1993. Metallogenesis in back-arc environments: The Lau Basin example. *Economic Geology*, **88** (8): 2154-2181.

Gena, K., Chiba, H., and Kase, K., 2005. Tin-bearing chalcopyrite and platinum-bearing bismuthinite in the active Tiger chimney, Yonaguni Knoll IV seafloor hydrothermal system, South Okinawa Trough, Japan. *Okayama University Earth Science Report*, **12** (1): 1-5.

Gena, K., Chiba, H., Kase, K., Nakashima, K., and Ishiyama, D., 2013. The tiger sulfide chimney, Yonaguni Knoll IV hydrothermal field, southern Okinawa Trough, Japan: The first reported occurrence of Pt-Cu-Fe-bearing bismuthinite and Sn-bearing chalcopyrite in an active seafloor hydrothermal system. *Resource Geology*, **63** (4): 360-370.

Glasby, G. P., and Notsu, K., 2003. Submarine hydrothermal mineralization in the Okinawa Trough, SW of Japan: An overview. *Ore Geology Reviews*, **23** (3-4): 299-339.

Guo, K., Zeng, Z., Chen, S., Zhang, Y., Qi, H., and Ma, Y., 2017. The influence of a subduction component on magmatism in the Okinawa Trough: Evidence from thorium and related trace element ratios. *Journal of Asian Earth Sciences*, **145**: 205-216.

Guo, K., Zhai, S., Yu, Z., Wang, S., Zhang, X., and Wang, X., 2018. Geochemical and Sr-Nd-Pb-Li isotopic characteristics of volcanic rocks from the Okinawa Trough: Implications for the influence of subduction components and the contamination of crustal materials. *Journal of Marine Systems*, **180**: 140-151.

Halbach, P., Pracejus, B., and Maerten, A., 1993. Geology and mineralogy of massive sulfide ores from the central Okinawa Trough, Japan. *Economic Geology*, **88** (8): 2210-2225.

Hannington, M. D., and Scott, S. D., 1988. Mineralogy and geochemistry of a hydrothermal silica-sulfide-sulfate spire in the caldera of axial seamount, Juan De Fuca Ridge. *Canadian Mineralogist*, **26**: 603-625.

Hannington, M. D., Jonasson, I. R., Herzig, P. M., and Petersen, S., 1995. Physical and chemical processes of seafloor mineralization at mid-ocean ridges. In: *Seafloor Hydrothermal System: Physical, Chemical, Biological, and Geological Interactions*. Humphris, S. E., *et al*., eds., American Geophysical Union, Washington, D. C., 115-157.

Hannington, M. D., Ronde, C. E. J. D., and Petersen, S., 2005. Sea-floor tectonics and submarine hydrothermal systems. In: *Economic Geology*, *100th Anniversary Volume*. Hedenquist, J. W., *et al*., eds., Society of Economic Geologists, Littelton, 111-141.

Hanor, J. S., 2000. Barite-celestine geochemistry and environments of formation. *Reviews in Mineralogy & Geochemistry*, **40** (1): 193-275.

Hodge, V., Stallard, M., Koide, M., and Goldberg, E. D., 1986. Determination of platinum and iridium in marine waters, sediments, and organisms. *Analytical Chemistry*, **58** (6): 616-620.

Humphris, S. E., and Bach, W., 2005. On the Sr isotope and REE compositions of anhydrites from the TAG seafloor hydrothermal system. *Geochimica et Cosmochimica Acta*, **69** (6): 1511-1525.

Humphris, S. E., and Thompson, G., 1978. Hydrothermal alteration of oceanic basalts by seawater. *Geochimica et Cosmochimica Acta*, **42** (1): 107-125.

Inagaki, F., Kuypers, M. M. M., Tsunogai, U., Ishibashi, J., Nakamura, K., Treude, T., Ohkubo, S., Nakaseama, M., Gena, K., Chiba, H., Hirayama, H., Nunoura, T., Takai, K., Jorgensen, B. B., Horikoshi, K., and Boetius, A., 2006. Microbial community in a sediment-hosted CO_2 lake of the southern Okinawa Trough hydrothermal system. *Proceedings of the National Academy of Sciences of the United States of America*, **103** (38): 14164-14169.

Jamieson, J. W., Hannington, M. D., Tivey, M. K., Hansteen, T., Williamson, N. M. B., Stewart, M., Fietzke, J., Butterfield, D., Frische, M., Allen, L., Cousens, B., and Langer, J., 2016. Precipitation and growth of barite within hydrothermal vent deposits from the endeavour segment, Juan de Fuca Ridge. *Geochimica et Cosmochimica Acta*, **173**: 64-85.

Judat, B., and Kind, M., 2004. Morphology and internal structure of barium sulfate-derivation of a new growth mechanism. *Journal of Colloid & Interface Science*, **269** (2): 341-353.

Kamenetsky, V. S., Binns, R. A., Gemmell, J. B., Crawford, A. J., Mernagh, T. P., Maas, R., and Steele, D., 2001. Parental basaltic melts and fluids in eastern Manus Backarc Basin: Implications for hydrothermal mineralisation. *Earth & Planetary Science Letters*, **184** (3): 685-702.

Kishida, K., Sohrin, Y., Okamura, K., and Ishibashi, J., 2004. Tungsten enriched in submarine hydrothermal fluids. *Earth & Planetary Science Letters*, **222** (3-4): 819-827.

Konno, U., Tsunogai, U., Nakagawa, F., Nakaseama, M., Ishibashi, J., Nunoura, T., and Nakamura, K., 2006. Liquid CO_2 venting on the seafloor: Yonaguni Knoll IV hydrothermal system, Okinawa Trough. *Geophysical Research Letters*, **33** (16): 627-642.

Kuhn, T., Herzig, P. M., Hannington, M. D., Garbe-Schönberg, D., and Stoffers, P., 2003. Origin of fluids and anhydrite precipitation in the sediment-hosted grimsey hydrothermal field North of Iceland. *Chemical Geology*, **202** (1-2): 5-21.

Lehuray, A. P., Church, S. E., Koski, R. A., and Bouse, R. M., 1988. Pb isotopes in sulfides from mid-ocean ridge hydrothermal sites. *Geology*, **16** (4): 362-365.

Li, S., Xu, J., and Luo, G., 2007. Control of crystal morphology through supersaturation ratio and mixing conditions. *Journal of Crystal Growth*, **304** (1): 219-224.

Marchev, P., Downes, H., Thirlwall, M. F., and Moritz, R., 2002. Small-scale variations of $^{87}Sr/^{86}Sr$ isotope composition of barite in the Madjarovo low-sulphidation epithermal system, SE Bulgaria: Implications for sources of Sr, fluid fluxes and pathways of the ore-forming fluids. *Mineralium Deposita*, **37** (6-7): 669-677.

Marumo, K., and Hattori, K. H., 1999. Seafloor hydrothermal clay alteration at Jade in the back-arc Okinawa Trough: Mineralogy, geochemistry and isotope characteristics. *Geochimica et Cosmochimica Acta*, **63** (18): 2785-2804.

Matsumoto, T., Kinoshita, M., Nakamura, M., Sibuet, J. C., Lee, C. S., Hsu, S. K., Oomori, T., Shinjo, R., Hashimoto, Y., Hosoya, S., Imamura, M., Ito, M., Tukuda, K., Yagi, H., Takekawa, K., Kagaya, I., Hokakubo, S., Okada, T., and Kimura, M., 2002. Volcanic and hydrothermal activities and possible 'segmentation' of the axial rifting in the westernmost part of the Okinawa Trough: Preliminary results from the Yokosuka/Shinkai 6500 Lequios cruise. *Journal of Deep Sea Research*, **19**: 95-107.

Matter, A., Peters, T., and Ramseyer, K., 1987. $^{87}Sr/^{86}Sr$-Verhältnisse und Sr-Gehalte von Tiefengrundwässern, Mineralien sowie Gesteinen us dem Kristallin und der Trias der Nord-schweiz. *Eclogae Geologicae Helvetiae*, **80** (2): 579-592.

Mcculloch, M. T., and Gamble, J. A., 1991. Geochemical and geodynamical constraints on subduction zone magmatism. *Earth & Planetary Science Letters*, **102** (3-4): 358-374.

Mottl, M. J., and Holland, H. D., 1978. Chemical exchange during hydrothermal alteration of basalt by seawater – I. Experimental results for major and minor components of seawater. *Geochimica et Cosmochimica Acta*, **42**: 1103-1115.

Noguchi, T., Shinjo, R., Ito, M., Takada, J., and Oomori, T., 2011. Barite geochemistry from hydrothermal chimneys of the Okinawa Trough: Insight into chimney formation and fluid/sediment interaction. *Journal of Mineralogical & Petrological Sciences*, **106** (1): 26-35.

Nunoura, T., and Takai, K., 2009. Comparison of microbial communities associated with phase-separation-induced hydrothermal fluids at the Yonaguni Knoll IV hydrothermal field, the Southern Okinawa Trough. *Fems Microbiology Ecology*, **67** (3): 351-370.

Paytan, A., Kastner, M., Martin, E. E., Macdougall, J. D., and Herbert, T., 1993. Marine barite as a monitor of seawater strontium isotope composition. *Nature*, **366** (6454): 445-449.

Paytan, A., Mearon, S., Cobb, K. M., and Kastner, M., 2002. Origin of marine barite deposits: Sr and S isotope characterization. *Geology*, **30** (8): 747-750.

Ray, D., Kota, D., Das, P., Prakash, L. S., Khedekar, V. D., Paropkari, A. L., and Mudholkar, A. V., 2014. Microtexture and distribution of minerals in hydrothermal barite-silica chimney from the Franklin Seamount, SW Pacific: Constraints on mode of formation. *Acta Geologica Sinica*, **88** (1): 213-225.

Sasaki, N., and Minato, H., 1983. Effect of the degree of supersaturation upon apparent partition coefficients of lead and strontium ions between $BaSO_4$ and aqueous solution. *Mineralogical Journal*, **11** (8): 365-381.

Seyfried, W. E., Seewald, J. S., Berndt, M. E., Ding, K., and Foustoukos, D. I., 2003. Chemistry of hydrothermal vent fluids from the main endeavour field, northern Juan de Fuca Ridge: Geochemical controls in the aftermath of June 1999 seismic events. *Journal of Geophysical Research – Solid Earth*, **108** (B9): 1-23.

Shikazono, N., 1994. Precipitation mechanisms of barite in sulfate-sulfide deposits in back-arc basins. *Geochimica et Cosmochimica Acta*, **58** (10): 2203-2213.

Shikazono, N., Kawabe, H., and Ogawa, Y., 2012. Interpretation of mineral zoning in submarine hydrothermal ore deposits in terms of coupled fluid flow-precipitation kinetics model. *Resource Geology*, **62** (4): 352-368.

Staude, S., Göb, S., Pfaff, K., Ströbele, F., Premo, W. R., and Markl, G., 2011. Deciphering fluid sources of hydrothermal systems: A combined Sr- and S-isotope study on barite (Schwarzwald, SW Germany). *Chemical Geology*, **286** (1-2): 1-20.

Suzuki, R., Ishibashi, J. I., Nakaseama, M., Konno, U., Tsunogai, U., Gena, K., and Chiba, H., 2008. Diverse range of mineralization induced by phase separation of hydrothermal fluid: Case study of the Yonaguni Knoll IV hydrothermal field in the Okinawa Trough Back-Arc Basin. *Resource Geology*, **58** (3): 267-288.

Tivey, M. K., and Delaney, J. R., 1986. Growth of large sulfide structures on the endeavour segment of the Juan de Fuca Ridge. *Earth & Planetary Science Letters*, **77** (3): 303-317.

Tivey, M. K., Olson, L. O., Miller, V. W., and Light, R. D., 1990. Temperature measurements during initiation and growth of a black smoker chimney. *Nature*, **346** (6279): 51-54.

Turcotte, D. L., and Brown, S. R., 1997. *Fractals and Chaos in Geology and Geophysics*. Cornell University, New York, 1-347.

Wang, S., Zhai, S., Yu, Z., Guo, K., and Zhang, X., 2018. Reflections on the model of modern seafloor hydrothermal system. *Earth Sciences*, **43** (3): 835-850 (in Chinese with English abstract).

Widanagamage, I. H., Schauble, E. A., Scher, H. D., and Griffith, E. M., 2014. Stable strontium isotope fractionation in synthetic barite. *Geochimica et Cosmochimica Acta*, **147**: 58-75.

Yang, K., and Scott, S. D., 1996. Possible contribution of a metal-rich magmatic fluid to a sea-floor hydrothermal system. *Nature*, **383** (6599): 420-423.

You, C. F., Castillo, P. R., Gieskes, J. M., Chan, L. H., and Spivack, A. J., 1996. Trace element behavior in hydrothermal experiments: Implications for fluid processes at shallow depths in subduction zones. *Earth & Planetary Science Letters*, **140** (1-4): 41-52.

Zeng, Z., Ma, Y., Chen, S., Selby, D., Wang, X., and Yin, X., 2017. Sulfur and lead isotopic compositions of massive sulfides from deep-sea hydrothermal systems: Implications for ore genesis and fluid circulation. *Ore Geology Reviews*, **87**: 155-171.

Zhang, L., Ren, Z. Y., Wu, Y. D., and Li, N., 2018a. Strontium isotope measurement of basaltic glasses by laser ablation multiple collector inductively coupled plasma mass spectrometry based on a linear relationship between analytical bias and Rb/Sr ratios. *Rapid Communications in Mass Spectrometry*, **32** (2): 105-112.

Zhang, X., Zhai, S., Yu, Z., Guo, K., and Wang, S., 2019a. Subduction contribution to the magma source of the Okinawa Trough – Evidence from boron isotopes. *Geological Journal*, **54**: 605-613.

Zhang, X., Zhai, S., Yu, Z., Yang, Z., and Xu, J., 2019b. Zinc and lead isotope variation in hydrothermal deposits from the Okinawa Trough. *Ore Geology Reviews*, **111**: 102944, https://doi.org/10.1016/j.oregeorev.2019.102944.

Zhang, X., Zhai, S., Yu, Z., Wang, S., and Cai, Z., 2018b. Mineralogy and geological significance of hydrothermal deposits from the Okinawa Trough. *Journal of Marine Systems*, **180**: 124-131.

Zierenberg, R. A., Koski, R. A., Morton, J. L., and Bouse, R. M., 1993. Genesis of massive sulfide deposits on a sediment-covered spreading center, Escanaba Trough, southern Gorda Ridge. *Economic Geology*, **88** (8): 2069-2098.

(Edited by Chen Wenwen)